

Alma Mater Studiorum Università di Bologna
Archivio istituzionale della ricerca

Northern Adriatic environmental changes since 500 AD reconstructed at Aquileia (Italy)

This is the final peer-reviewed author's accepted manuscript (postprint) of the following publication:

Published Version:

Kaniewski, D., Marriner, N., Sarti, G., Bertoni, D., Marchesini, M., Rossi, V., et al. (2022). Northern Adriatic environmental changes since 500 AD reconstructed at Aquileia (Italy). QUATERNARY SCIENCE REVIEWS, 287, 107565-107577 [10.1016/j.quascirev.2022.107565].

Availability:

This version is available at: <https://hdl.handle.net/11585/893684> since: 2022-09-08

Published:

DOI: <http://doi.org/10.1016/j.quascirev.2022.107565>

Terms of use:

Some rights reserved. The terms and conditions for the reuse of this version of the manuscript are specified in the publishing policy. For all terms of use and more information see the publisher's website.

This item was downloaded from IRIS Università di Bologna (<https://cris.unibo.it/>).
When citing, please refer to the published version.

(Article begins on next page)

This is the final peer-reviewed accepted manuscript of:

Kaniewski, David; Marriner, Nick; Sarti, Giovanni; Bertoni, Duccio; Marchesini, Marco; Rossi, Veronica; Lena, Anna; Bivolaru, Alexandra; Pourkerman, Majid; Vacchi, Matteo; Cheddadi, Rachid; Otto, Thierry; Luce, Frédéric; Cottica, Daniela; Morhange, Christophe: *Northern Adriatic environmental changes since 500 AD reconstructed at Aquileia (Italy)*

QUATERNARY SCIENCE REVIEWS, vol. 287 ISSN 0277-3791

DOI: 10.1016/j.quascirev.2022.107565

The final published version is available online at:

<https://dx.doi.org/10.1016/j.quascirev.2022.107565>

Rights / License:

The terms and conditions for the reuse of this version of the manuscript are specified in the publishing policy. For all terms of use and more information see the publisher's website.

This item was downloaded from IRIS Università di Bologna (<https://cris.unibo.it/>)

When citing, please refer to the published version.

Northern Adriatic environmental changes since 500 AD reconstructed at Aquileia (Italy)

David Kaniewski^{1,2}, Nick Marriner³, Giovanni Sarti⁴, Duccio Bertoni⁴, Marco Marchesini⁵,
Veronica Rossi⁶, Anna Lena⁷, Alexandra Bivolaru⁸, Majid Pourkerman⁹, Matteo Vacchi¹⁰,
Rachid Cheddadi¹¹, Thierry Otto¹², Frédéric Luce¹², Daniela Cottica¹³, Christophe Morhange^{8,14}

¹TRACES, UMR 5608 CNRS, Université Toulouse Jean Jaurès, Maison de la Recherche, 5 allées A. Machado 31058 Toulouse Cedex 9, France

²Département de Biologie et Géosciences, Université Paul Sabatier - Toulouse 3, Toulouse cedex 9, France

³CNRS, ThéMA, Université de Franche-Comté, UMR 6049, MSHE Ledoux, 32 rue Mégevand, 25030 Besançon Cedex, France

⁴Dipartimento Scienze della Terra - Università di Pisa, Via S. Maria 53 - 56126 Pisa, Italy

⁵Palynology and Archaeobotany Laboratory - C.A.A. Giorgio Nicoli Headquarters: via Marzocchi, 17 40017 San Giovanni in Persiceto (Bologna), Italy

⁶Dipartimento di Scienze Biologiche, Geologiche e Ambientali. Università di Bologna, Italy

⁷Université de Perpignan Via Domitia, Centre de Recherches sur les Sociétés et Environnements en Méditerranées (CRESEM, UR 7397), 52 avenue Paul Alduy, 66860 Perpignan cedex 9

⁸Aix Marseille Université, CNRS, IRD, INRA, Collège de France, CEREGE, Aix-en-Provence, France

⁹INIOAS (Iranian National Institute for Oceanography and Atmospheric Sciences), No. 3, Etemad Zadeh St., Fatemi Avenue, Tehran, Iran

¹⁰Dipartimento di Scienze Della Terra, Università di Pisa, Pisa, Italy

¹¹Université Montpellier II, CNRS-UM-IRD, ISEM, France

¹²Laboratoire Ecologie Fonctionnelle et Environnement, Université de Toulouse, CNRS, INP, UPS Toulouse cedex 9, France

¹³Dipartimento di Studi Umanistici, Università Ca' Foscari Venezia, Palazzo Malcanton - Marcorà, Dorsoduro 3484/D, I-30123 Venezia, Italy

¹⁴EPHE-Section des Sciences Historiques et Philologiques, AOROC, UMR 8546 - Archéologie et Philologie d'Orient et d'Occident, CNRS/PSL, École normale supérieure, 45 rue d'Ulm, 75230 Paris Cedex 5, France

Corresponding author: David Kaniewski

Email: david.kaniewski@univ-tlse3.fr

Highlights

- Palaeoecological study of Aquileia, the ninth city of the Roman Empire
- Insights into the ecosystem dynamics for the post-Roman period
- Climate pressures shaped ecosystem dynamics
- Anthropogenic activities acted as secondary pressures
- Late Antique Little Ice Age was the coolest and driest episode recorded

Abstract

The fluvial harbour of Aquileia (Italy), one of the most important Roman trading centres in the Mediterranean, was abandoned after the city's destruction in 452 AD. The deserted harbour evolved into a swamp surrounded by a floodplain that has recorded the anthropogenic, environmental and climatic pressures that have occurred during the last 1500 years in the northern Adriatic. Focusing on the period since 500 AD, we here reconstruct the area's long-term ecosystem dynamics. We show that ecosystem dynamics mainly mirror the climate phases of the pre-industrial era. After the Roman era, anthropogenic activities (agriculture, pasture and fire activity) declined in scope and amplitude and are chronologically limited (from the late 7th to the early 13th centuries AD), acting as a background pressure on ecosystems. The main non-human impacts recorded by ecosystems correspond to the Late Antique Little Ice Age, defined by an average temperature anomaly of $-2.04 \pm 0.17^{\circ}\text{C}$, exceeding the Pre-industrial Little Ice Age by $-1.26 \pm 0.16^{\circ}\text{C}$ in severity. The temperatures reconstructed for the Medieval Climate Anomaly are close to those recorded for the 20th century AD (average anomaly of $0.08 \pm 0.15^{\circ}\text{C}$) but they differ from the 21st century AD, according to the CRUTEM4 data. Aquileia shows that ancient harbours are key areas to understand how climate and human societies have shaped northern Adriatic environments since the post-Roman period.

Keywords

Aquileia, Fluvial harbour, Ecosystems, Anthropogenic activities, Climate, Late Holocene, Italy

1. Introduction

The reconstruction of long-term environmental dynamics from ancient harbours has highlighted the importance of bio- and geo-sciences in understanding coastal man-made environments resulting from the Mediterranean's long and rich maritime history (*e.g.* Marriner and Morhange, 2007; Marriner et al., 2014). In Italy, numerous seaports and associated fluvial harbours have been intensively studied, providing an in-depth understanding of the human activities and anthropogenic pressures on environments since the emergence and development of these port complexes. Harbours such as *Altinum*-Venice (Ninfo et al., 2009), *Portus Lunae*-Luni (Bini et al., 2012), *Portus*-Rome (Sadori et al., 2010, 2015 ; Mazzini et al., 2011), *Ostia*-Rome (Salomon et al., 2018), *Neapolis*-Naples (Allevato et al., 2010 ; Di Donato et al., 2018), *Portus Pisanus*-Pisa (Kaniewski et al., 2018) or Pisa S. Rossore (Mariotti Lippi et al., 2007; Bini et al., 2015) have furnished key information on how human societies have shaped long-term landscape dynamics. While most studies have focused on the harbour phase, few analyses have focused on the post-harbour period, when structures were abandoned and anthropogenic pressures decreased or even disappeared (*e.g.* Marriner and Morhange, 2006; Morhange et al., 2016).

Lying on the border between the Friuli plain and the edges of the Grado lagoon (Fig. 1), Aquileia, a Roman colony founded in 181 AD, and a UNESCO site since 1998, was located in a highly dynamic natural environment shaped by fluvial activity (Arnaud-Fassetta et al., 2003). Fresh, brackish and sea waters alternatively presented opportunities and risks for local communities and the site has been the object of long-term archaeological investigations and projects. During the Roman period, Aquileia was the focus of a communication network, consisting of terrestrial routes implemented by a system of natural and artificial waterways which provided access to the sea and maritime trade routes (Cottica and Ventura, 2019). The city soon became the most important trading centre (glass, wine, oil, olives, wool, gold and spices) of the northern Adriatic area (Zaccaria and Pesavento Mattioli, 2009). By the 1st century AD, Aquileia had become a thriving centre, a major emporium in the Mediterranean and the Adriatic Sea, and a key site in commercial routes, lying at a crossroads for trade goods transiting from the Mediterranean Sea to the Danube provinces (Carre, 2008; Maggi et al., 2017). Furthermore, the site played a key role in Roman imperial political and military history: from the age of Marcus Aurelius onwards, it withstood several attacks until it fell under the siege of Attila in 452 AD, following the invasion of the Huns. Subsequently, Aquileia lost its importance for ~200 years before regaining its status as the region's principal city in the 7th century AD

with the rise of patriarchal rule. Aquileia gradually declined during the 15th century due to the increasing power of the Republic of Venice (Capulli, 2013).

Despite its important historical status, few environmental studies have been undertaken at Aquileia (Arnaud-Fassetta et al., 2003, 2010; Siché et al., 2004), one of the most significant fluvial harbours of the Roman Empire (Carre, 2008; Cottica et al., 2018; Cottica and Ventura, 2019). The geographical location of the city, however, makes it a key area to probe the environmental transitions that have occurred over the past centuries in the northern Adriatic coastal plain.

Here we investigate the post-Roman ecosystem dynamics of Aquileia to i) reconstruct how the environments have evolved during the last 1500 years, ii) investigate the major tipping points in ecosystem dynamics and iii) probe the environmental and climate forcing factors. Using a fossil record, we provide an in-depth ecological study of the area, reconstructing the major vegetation changes and their evolution through time. We also furnish a pollen-based climate reconstruction to identify the climate changes during the pre-industrial era [Late Antique Little Ice Age (LALIA), Medieval Climate Anomaly (MCA), and Pre-industrial Little Ice Age (LIA)]. Aquileia shows that harbours are key areas to understand how the Mediterranean environment was shaped by both human societies and natural factors during recent centuries.

2. Present-day vegetation

The area is located at the boundary of the Mediterranean belt. Though extensively transformed by human activities, nowadays, the vestiges of the fluvial harbour area are surrounded by patches of *Quercus robur*, *Carpinus betulus*, *Crataegus monogyna*, *Ligustrum vulgare* and *Cornus sanguinea* with man-made stands of *Pinus pinea* and *Cupressus sempervirens* along the old quays. Several species of *Prunus* (*P. domestica*, *P. avium*, *P. mahaleb*, *P. spinosa*) develop in the adjacent areas. The riparian vegetation is composed of rare patches of *Salix alba*, *Populus alba* and *Alnus glutinosa* along with a dense wet meadow composed of *Filipendula ulmaria*, *Agrostis stolonifera*, *Phragmites* sp. and a Magnocaricion (including *Carex* sp., *Cyperus* sp., *Mentha aquatica* and *Sagittaria* sp.).

3. Material and methods

3.1. The core

Biological indicators were extracted from the 450-cm Aquileia core III (AQ III) drilled in the ancient Roman harbour (45°46'29.068"N, 13°22'10.376"E, 1 m a.s.l.) during a field campaign in 2020 (Fig. 1). The grain-size analysis was performed with H₂O₂ treatment and removal of organic matter. Only the granular fraction was analysed. The lithology of the core AQ III is organized as follows: the bottom two meters (450-250 cm) comprise sandy deposits overlain by 142 cm of silt, organic silt and peat (250-108 cm). The upper levels correspond to a silty-sandy matrix (108-0 cm; Fig. 2). No evidence of stratigraphic hiatuses was observed in the core or laboratory data. The core was sampled every 2 cm on average. Bioindicators are only well-preserved in the silt-organic-peat layers.

3.2. Chronology

The chronology of the core AQ III (Fig. 2) is based on seven accelerator mass spectrometry (AMS) ¹⁴C dates performed on short-lived samples (small leaves) at 110 cm (200±30 ¹⁴C yr BP), 126 cm (270±30 ¹⁴C yr BP), 156 cm (380±30 ¹⁴C yr BP), 166 cm (470±30 ¹⁴C yr BP), 204 cm (1260±30 ¹⁴C yr BP), 232 cm (1490±30 ¹⁴C yr BP), and 246 cm (1540±30 ¹⁴C yr BP). Aquatic remains were excluded, and all of the botanical macro-remains sent to Beta Analytic (Florida) comprised small leaves from deciduous vegetation. The ¹⁴C dates were calibrated to 2 sigma (σ) using Calib Rev 8.0.1 (IntCal20). All the calibrated ages are denoted in AD, consistent with the historical data. The age-depth model is based on a linear interpolation between each of the intercepts (and the 2σ). The interpolation is compared with a linear model and a polynomial model in order to estimate the difference between the two signals (Fig. 2). Sediment compaction during coring was calculated in order to obtain the real depth of each deposit. Subsequently, the sedimentation rate between each ¹⁴C date was calculated (Fig. 2). Because samples were taken at regular intervals along the 250-cm sediment column, the chronological resolution is directly dependent on the sedimentation rate (Fig. 2).

3.3. Biological data

Samples from the core AQ III were prepared for pollen analysis using standard procedures for clay-silt samples (fully detailed in Faegri and Iversen, 1989). Pollen grains were counted under

x400 and x1000 magnification using an Olympus microscope. Pollen frequencies (expressed as percentages) are based on the terrestrial pollen sum, excluding local helophytes, macrophytes and spores of non-vascular cryptogams. Aquatic taxa frequencies were calculated by adding the local helophytes-macrophytes to the terrestrial pollen sum. The mean pollen sum was 507 ± 145 pollen grains, with a minimum of 240 pollen grains (there were only five samples with less than 300 pollen grains). The median value was 547 pollen grains, with a 25th percentile of 383 pollen grains and a 75th percentile of 627 pollen grains. The mean number of taxa was 59 ± 5 taxa, with a minimum of 42 taxa. The median value was 60 taxa, with a 25th percentile of 58 taxa, and a 75th percentile of 63 taxa. The palynological data are presented as a detailed pollen diagram in Fig. 3. The river floodplain vegetation is shown as a second detailed pollen diagram (Fig. 4).

To support the identification of the main environmental changes along the core, sixteen samples were also collected for qualitative analysis of the ostracod fauna with a resolution of <15 cm. Samples were prepared adopting the standard methodology (e.g. Amorosi et al., 2013) and the taxonomic identification was based on Henderson (1990).

3.4. Statistical analyses

Statistical analyses were performed using XI-Stat²⁰¹⁹ (<https://www.xlstat.com>), R 4.1.0 (R Core Team, 2021) and the software package PAST 4.08 (Hammer et al., 2001). All the long-term trends were calculated using a polynomial model (order 5 - lowest standard deviation, $P_{\text{value}} < 0.001$; the R^2 is mentioned on each graph). Pollen data were studied using a cluster analysis (descending type; Fig. 5) to calculate a dendrogram, using branches as ecological distances between groups of taxa. The test was performed using Paired group as algorithm and Correlation as the similarity measure. Each cluster was summed to generate pollen-derived vegetation patterns (PdVs) and assigned to a potential location, from the dryland to the floodplain, referring to modern patches of vegetation (Fig. 5). The riparian forest (fen trees) was added to the marshland plants (macrophytes and helophytes) to create a curve reflecting the floodplain dynamics (Fig. 6A). A principal component analysis (PCA) was subsequently performed to test the ordination of samples by assessing major changes in the PdV-scores. The first axis (PCA-Axis 1), which carries the maximum variance (77% of total variance), was extracted. The PdVs influenced by the floodplain are loaded by the positive PCA-Axis 1 scores while the PdVs located beyond the influence of the river are loaded by the negative scores. A regular chronological interpolation (10-yr) was applied to the dataset in order to reduce biases

linked to chronological gaps, particularly at the bootstrap level. We then transformed the PCA-Axis1 scores using a Loess smoothing (with a LOWESS algorithm) and performed a bootstrap to estimate a 95% confidence band based on 1000 random replicates. The Loess curve and the 95% confidence band were used as a proxy for the floodplain dynamics (Fig. 6B). The cultivated species and pasture activities were added to test their occurrences in a context of long-term floodplain changes (Fig. 6C).

Variations in the floodplain (fen trees, helophytes and macrophytes) were further contrasted with the dynamic of the dry floodplain scrubs, using both a synthetic diagram and a Kernel density 2D model (with Gaussian as function; Fig. 7A). The two time-series were then tested using a cross-correlation ($P_{\text{value}} < 0.001$; the R^2 value is indicated on Fig. 7A). The floodplain dynamics (fen trees and helophytes) were subsequently compared to the dryland components (pine-oak woodland cluster), using both a synthetic diagram and a Generalized Linear Model (Fig. 7B). The two time-series were also tested using a cross-correlation ($P_{\text{value}} < 0.001$; the R^2 value is indicated on Fig. 7B). A Gradient Species Packing test was finally added to identify the distribution of each cluster, using the floodplain as a stationary reference (Fig. 7C).

3.5. Agriculture, pasture activities and fire

Agriculture activities are mainly based on cereals (Poaceae cerealia) with a diversified arboriculture comprising grapevines (*Vitis vinifera*), olive trees (*Olea europaea*), walnut trees (*Juglans regia*) and diverse Rosaceae (*Prunus* sp.). Pasture activities are identified by various genera such as knapweed (*Centaurea*), plantain (*Plantago*), knotweed (*Polygonum*) and sorrel (*Rumex*). To identify human impacts, a pasture activities/agriculture ratio was calculated (Fig. 8A). All the long-term trends were calculated using a polynomial model (order 5, $P_{\text{value}} < 0.001$).

The fire history of Aquileia was reconstructed by counting charcoal particles (50-200 μm) on the pollen slides. The 50 μm size criterion was chosen to avoid confusion between microscopic charcoal fragments and opaque minerals, which are typically $< 50 \mu\text{m}$ (Parshall and Foster, 2002; Pederson et al., 2005). We adopted the 200-300 items (sum of charcoal particles) defined by Finsinger and Tinner (2005). A first charcoal concentration curve (fragments per cm^{-3}) was drawn according to a linear age-scale (Fig. 8A). The fire activity was compared with the ratio pasture activities/agriculture, with the dynamics of the mixed oak forest (Fig. 8B), and with agricultural activities (Fig. 8C). Charcoal concentrations were converted into charcoal accumulation rates (CHAR) based on the sedimentation rate estimated by the age-depth model

(Fig. 8D). These analyses were performed in R using R-PaleoAnomalies (<https://github.com/wfinsinger/R-PaleoAnomalies>), a code which builds on CharAnalysis. The analysis comprised the following steps: i) The CHAR record was resampled to equal time intervals (20-yr) using a window corresponding to the mean sedimentation rate of the record, ii) the data were log-transformed to homogenize variance, iii) the “Background Component” was estimated with a local polynomial (100-yr moving window), facilitating the calculation of the “Peak Component”, and iv) fire episodes were detected using a threshold within the range of values with the lowest sensitivity to the number of peaks detected, derived by plotting a frequency distribution histogram of the peak component. The process is fully described in the literature (Long et al., 1998; Higuera et al., 2008, 2009; Doyen et al., 2015).

3.6. Pollen-derived climate reconstruction

The pollen-based model used to reconstruct climate variables (Fig. 9) has been described extensively in the literature (Cheddadi and Khater, 2016; Cheddadi et al., 2016, 2017) and has been shown to provide coherent climate reconstructions (e.g., Kaniewski et al., 2019, 2020, 2021). Past climate variables were derived from the Aquileia fossil pollen record. We assigned the pollen taxa of Aquileia to modern plant species based on our knowledge in palynology, botany, and ecology. Edaphic, aquatic, human-related, or less than 1% of the total pollen taxa were not considered in the climate reconstruction. For each fossil sample, we used the weighted median of each pollen taxon identified in individual fossil samples, using the percentages of pollen as weights to calculate the median of all pollen taxa. The uncertainty of the reconstruction for each fossil sample is estimated by omitting one taxon from each iterative estimate, as many times as the number of taxa in the fossil sample. This quantification method assumes that the modern climatic range of a species encompasses its range during the studied time span and that the closer the best climatic value is to the area where it is most abundant, the more abundant it is (Cheddadi et al., 2021). Helophytes, macrophytes and spores of non-vascular cryptogams were excluded from the matrix. All reconstructions are shown with their estimated errors (Fig. 9), and with their long-term trends based on a polynomial model (order 5, $P_{\text{value}} < 0.001$; the R^2 is shown on each graph). The temperature anomalies are based on the annual average for the control period 1961-1990 (13.04°C; Fig. 9A). Temperature anomalies were first compared with the loess-smoothed PCA-Axis 1 (Fig. 9B) and the spring-summer precipitation (Fig. 9C). The 1850-2019 CRUTEM data (Osborn and Jones, 2014) were then added to test the reliability of the temperature reconstruction from core AQ III (Fig. 9D). A

sinusoidal model was applied ($P_{\text{value}} < 0.001$) to link data from core AQ III with CRUTEM4 (Fig. 9D).

4. Results

4.1. Lithology and chronology

The lower part of the core AQ III, corresponding to an abandoned channel of Roman age, was completely void of bioindicators. The sandy matrix was not conducive to the conservation of ostracods, pollen and other non-palynomorphs. The overlying levels, which correspond to silt, organic silt and peat deposits (Fig. 2), were found to be rich in palynomorphs, with an average of 507 ± 145 pollen grains counted per sample and an average concentration of 2027 ± 585 pollen per cm^{-3} . The median value is 2186 pollen per cm^{-3} with a 25th percentile of 1531 pollen per cm^{-3} and a 75th percentile of 2506 pollen per cm^{-3} . Within this interval, hypohaline ostracods are locally found although represented by few valves. The sedimentation rate (SR) varies according to the lithology. While the lower silty layers have a SR of 1.7 to 2 mm per year, the organic silt and peat deposits are characterized by lower rates of 0.5 mm per year (Fig. 2). The upper silty layers are characterized by a SR of 1.25 to 2 mm per year, close to the values recorded for the lower layers. The uppermost level corresponds to a silty-sandy matrix completely sterile of bioindicators. The material used for ^{14}C dating was only found in the silt-organic and silt-peat layers. No macro-remains were observed in the lower sandy matrix and upper silty-sand deposits. The core AQ III is framed by a chronology spanning from 510 ± 85 AD to 1770 ± 40 AD (Fig. 2), or from the Ostrogothic Kingdom to the Austrian Empire.

4.2. Ecosystem dynamics

Since 500 AD, the evolution of vegetation surrounding the waterlogged area developed after the abandonment of the Roman fluvial harbour is detailed in two pollen diagrams with the first focused on terrestrial plants (Fig. 3) and the second on floodplain vegetation (Fig. 4). The pollen dataset was categorized into 9 PdVs grouped into 4 assemblages (Dryland, Dry floodplain, Wetland, Floodplain) using a cluster analysis (Fig. 5). The PdVs were then converted into markers of hydrological shifts using the floodplain vegetation (Fig. 6A) and a Loess PCA-Axis 1 (Fig. 6B) as proxies. The outcomes suggest a humid environment until 660 ± 55 AD, with a well-developed floodplain (macrophytes and helophytes) surrounded by fen trees (*Alnus*,

Betula, *Populus* and *Salix*) and by a wet meadow (dominated by Poaceae, Ranunculaceae and Campanulaceae). Most of the macrophytes and helophytes suggest the presence of stagnant waters or a river branch with a very low streamflow, creating a swamp in the city. This interpretation is consistent with the occurrence of ostracods typical of shallow hypohaline environments with stagnant waters (*Pseudocandona* and *Cyclocypris* species). Two spikes at 565-590±55 AD may be consistent with floodplain high-stands (Fig. 6A). Agriculture was weakly developed during this first phase (Fig. 6C). After 660±55 AD, the floodplain regressed significantly, reaching its first low level at 950±45 AD and a second at 1200-1230±35 AD (Fig. 6). The macrophytes and helophytes were gradually replaced by dry floodplain scrubs (Fig. 7A) and by a pine-oak woodland (Fig. 7B), suggesting the development of drier environmental conditions. Accordingly, the disappearance of ostracods points to a marked decrease in the water table. A reliable linear relationship ($R^2=0.66$; $P_{\text{value}} < 0.001$) was established between the loss of fen trees and helophytes, and the increase of pine-oak woodland, implying an inverse relationship. During this period (660±55 to 1230±35 AD), agriculture and pastoral activities increased significantly (Fig. 6C). From 1230±35 to 1770±40 AD, the area oscillates between dry and wet conditions, suggesting unstable environmental conditions. The drier phases are supported by xeric components (*e.g.* Chenopodiaceae, *Artemisia*, Asteraceae, *Quercus* evergreen). The wet phases, consistent with a rise in the floodplain's water table, are attested by an increase in helophytes and wet meadow plants (Fig. 4), and the local reappearance of a hypohaline ostracod fauna. After 660±55 AD, and the drying of the swamp, wet phases were recorded at 1000-1050±40, 1250-1310±35, 1380-1420±25, 1480-1500±40, and 1590-1650±30 AD (Fig. 6A-B). After 1200±35 AD, agricultural and pastoral activities declined sharply, then fluctuated, before regaining in importance after 1710±35 AD (Fig. 6C).

4.3. Agricultural practices, pastoral activities and fire

The agricultural practices (agri- and arboriculture) and pastoral activities were first depicted as long-term dynamics (Fig. 6C) and then shown as ratios (Fig. 8A). During the last 1500 years, agriculture has never exceeded 15% of the pollen sum (with a maximum of 6% for the cereals) and the pastoral plants never rise above 12%. Both were probably more developed during the Roman period and the heydays of the city. Agriculture is mainly recorded from 620±55 to 1230±35 AD, during the patriarchal rule of the city, and then after 1710±35 AD, during the Austrian Empire (Fig. 8A). Fire activity meshes inversely with the mixed oak forest phase (Fig. 8A). The mixed oak forest regressed most significantly when fire return intervals were high,

and inversely developed when slash-and-burn agriculture declined (Fig. 8B). When both agricultural and pastoral practices are combined, there is a clear link between anthropogenic activities and ignitions, suggesting human-induced fires in the area (Fig. 8C and 8D). From 1230 \pm 35 to 1430 \pm 35 AD, a period marked by general decline in anthropogenic and cultivated taxa, the pastoral activities/agriculture ratio shows a prevalence of pastoral activities over agriculture (Fig. 8A). After 1710 \pm 35 AD, a declining ratio is consistent with a renewed increase in agricultural activities (Fig. 8A), probably slash-and-burn agriculture as fire indicators also increase (Fig. 8D).

4.4. Climate reconstruction

The reconstruction of temperature anomalies since 500 AD depicts colder periods centred on the LALIA, the Oort minimum, and the different episodes of the LIA (Wolf minimum, Spörer minimum, Maunder minimum; Fig. 9A; Marriner et al., 2022). The colder phase corresponds to the LALIA, locally recorded from 535 \pm 75 to 660 \pm 55 AD, with a minimum of -3.5 \pm 0.17°C at 590 \pm 55 AD and an average of -2.04 \pm 0.17°C for the whole phase. The second cooler period corresponds to the Maunder episode, with a minimum of -1.4 \pm 0.14°C and an average of -0.78 \pm 0.15°C for the whole phase. The cold periods are correlated with greater humidity and the expansion of the swamp area, as highlighted by the Loess PCA-Axis 1. An exception is the Maunder minimum, during which the area remained dry (Fig. 9B). Focusing on spring-summer precipitation, the drier phases are centred on the Medieval Climate Anomaly (average 291 \pm 2 mm), and on the period lasting from the end of the Wolf minimum to the onset of the Maunder minimum (average 287 \pm 2 mm; Fig. 9C). While precipitation increases are concomitant with the development of the swamp area, the Maunder minimum is characterized by higher rainfall but a dry context (Fig. 9B).

When the reconstructed temperature anomalies are compared and contrasted with the CRUTEM4 dataset (1850-2019 AD; Jones et al., 2012; Osborn and Jones, 2014), there is a clear link between the record from Aquileia and the climatic evolution of the northern Adriatic. The anomalies of -1.09 \pm 0.14°C at 1770 \pm 40 AD (last point recorded in the core AQ III) and of -1.13°C at 1850 AD (first data available in the CRUTEM4 dataset) are consistent. The sinusoidal model ($P_{\text{value}} < 0.001$) shows no discontinuity between the two curves (Fig. 9D), suggesting that core AQ III and CRUTEM4 are comparable. It also appears that the MCA was not warmer than the 20th century AD in the northern Adriatic, but cooler compared to the 21st century AD.

5. Discussion

The fluvial harbour of Aquileia offers a rare record of the environmental shifts that have occurred on the northern Adriatic coastal plain since 500 AD. In the Gulf of Venice, the late Holocene ecosystem dynamics have been poorly studied, especially the last two millennia. Previous work has focused on the dynamics of salt-marsh plant communities (Miola et al., 2010), on long-term sequences covering the Pleistocene-Holocene (*e.g.* Bortolami et al., 1977; Bondesan et al., 2003; Masari et al., 2004; Pini et al., 2009; Donnici et al., 2012), on grasslands covering the eastern part of the northern Adriatic (Kaligarič et al., 2006), and on sequences from the Istrian Peninsula, Croatia (*e.g.* Kaniewski et al., 2016, 2021).

5.1. A wet and cold LA Little Ice Age

From 508±80 to 660±55 AD, Aquileia was wet, marked by significant occurrences of fen trees, helophytes, macrophytes and by an expanded wet meadow. The floodplain that hosted the city of Aquileia was well-developed during the Ostrogothic Kingdom and the early phase of the Kingdom of the Lombards. The zone was a swamp area, characterized by low-energy fluvial dynamic in the center surrounded by stagnant water. The background vegetation is mainly composed of a mixed oak forest and by short incursions of dry floodplain scrubs. The upper part of the marine core RF 93-30, from the western flank of the Adriatic (Oldfield et al., 2003) depicts a similar vegetation pattern, with a dominant mixed oak forest and a strong presence of helophytes (Cyperaceae). At Aquileia, two major wet peaks at 565-590±55 AD may suggest a floodplain high stand (Fig. 6A). Similar conclusions were reached by a geomorphological study of the Natiso River (Siché, 2008). As agriculture and pastoral activities were weakly developed in the northern Adriatic (Fig. 6C), the environmental variations seem to be mainly related to climate. The LALIA is defined as a cold episode which lasted from 536 to 660 AD. Some studies suggest that it exceeded the LIA in severity (Büntgen et al., 2016), with a major impact in Italy (Neukom et al., 2019; Peregrine, 2020). The reconstructed temperatures at Aquileia show a similar pattern, with an average of -2.04±0.17°C for the LALIA, and an average of -0.78±0.15°C for the coldest event of the LIA (Maunder minimum). The minima follow the same trend, with a value of -3.5±0.17°C at 590±55 AD (LALIA) and -1.4±0.14°C at 1642±30 AD (LIA; Fig. 9A). The LALIA at Aquileia was, on average, approximately -1.26°C colder than the LIA. A wetter and colder climate, as shown by the core AQ III (Fig. 9C), has also been

elucidated in the Gulf of Gaeta (Di Rita et al., 2018), in Sicily (Sadori et al., 2016) and in coastal Croatia where spring-summer precipitation increased significantly during this phase (Kaniewski et al., 2021). At other sites, this period is inversely associated with a marked human impact on the environment (e.g. Lago Lungo; Mensing et al., 2015; core ND2; Michelangeli et al., 2022). The core AQ III suggests a cold and wet northern Adriatic from 508±80 to 660±55 AD consistent with Mediterranean Sea Surface Temperatures at this time (Marriner et al., 2022).

5.2. A shift towards warmer and drier conditions

From 660±55 to 1230±55 AD, the area changed radically from a floodplain to a drier environment as shown by the Loess PCA-Axis1 (Fig. 6B), with an important extension of the scrubs on desiccated banks, and of the pine-oak woodland in adjacent areas. The Natiso River was transformed into a minor waterway with reduced flow. One of the main changes since 660±55 AD was the development of agriculture during the patriarchal rule of the city. Fire has long been an element of pressure on ecosystems and an agent associated with agricultural activities in Italy (e.g. Sadori and Giardini, 2007; Vanni re et al., 2008). At Aquileia, the same pattern was found, but agriculture was however limited as taxa associated with anthropogenic activities never exceed 15% of the pollen sum during this period. The olive trees never reached values equivalent to those recorded at the Lago Alimini Piccolo in southern Italy (Di Rita and Magri, 2009) and are closer to the values identified at Lago Lungo (Mensing et al., 2015) and in the core ND2 (Michelangeli et al., 2022). Similarly, fire events are mainly recorded during the reintroduction of cultivated species (Fig. 8D), a short period extending from 660±55 to 750±55 AD and after 1700 AD. The development of slash-and-burn agriculture, while limited, seems to have mainly affected the mixed oak forest, freeing up ecological niches colonized by the pine-oak woodland (Fig. 7B). As agriculture was not dominant in the area, the variations recorded by the core AQ III derive from a mixed climate-anthropogenic signal, with an environmental forcing more influential than anthropogenic factors as suggested by the occurrence of the main climatic phases of the pre-industrial era. Focusing on the climate parameters, it appears that the area was warmer after the LALIA, with a first cooler period corresponding to the Oort minimum (from 1000±40 to 1050±40 AD; Fig. 9A). The Oort minimum, defined as a period of low solar activity (Yiou et al., 2012), does not seem to have been a major event in the northern Adriatic, with an average of -0.2±0.14 C recorded at Aquileia. The weak influence of the Oort minimum in the Gulf of Venice has already been

highlighted with regards to sea-storm activity (Camuffo et al., 2000). After 1050±40 AD, the area around Aquileia became warmer, with temperature anomalies peaking at 0.4±0.15°C at 1135±35 AD. While the MCA (core period: 1000-1200 AD) is characterized by anomalously warm conditions in some (but not all) regions (Mann et al., 2009; Lüning et al., 2019), in the northern Adriatic, the average temperature anomaly for the whole episode is 0.08±0.15°C, close to the control period 1961-1990 AD (13.04°C). This observation is corroborated by a European study which revealed that temperatures during the MCA were probably as warm as the 20th century AD (Büntgen and Tegel, 2011). The MCA at Aquileia ended at 1230-1250±35 AD. AQ III shows a warm and dry northern Adriatic from 660±55 to 1230-1250±35 AD, with a low impact of the Oort minimum and a local, limited, increase of anthropogenic pressures on the environment.

5.3. A succession of cold and warm phases

From 1250±35 to 1770±40 AD, the swamp area oscillated between wet and dry phases. The dry phases are attested by the occurrence of xeric components within and beyond the floodplain while the wet episodes are mainly attested by an increase in helophytes and wet meadow plants. This suggests that the flow of Natiso River has oscillated markedly over time (Fig. 6A). Although the wet phases are clearly identified by the Loess PCA-Axis1, the waterbody never reached the level recorded during the LALIA. Following the end of patriarchal rule (in 1236 AD), agricultural, pastoral and fire activities decreased markedly. All the anthropogenic pressures on ecosystems seem to have been reduced until 1710±35 AD and renewed after this period (Fig. 6C). The signal is thus mainly modulated by environmental factors, namely climate variations. The first cold and wet phase occurred from 1250±35 to 1335±30 AD and meshes with the Wolf minimum, a Grand Solar Minimum spanning the period 1270-1350 AD (Steinhilber et al., 2009; Usoskin et al., 2016; Fogtmann-Schulz et al., 2021). At Aquileia, the temperature anomaly recorded during this phase is on average -0.32±0.16°C. The area became colder but also wetter, with a clear positive deviation of the spring-summer precipitations, similar to the trends observed in coastal Croatia (Kaniewski et al., 2021). The second cold and wet phase occurred from 1460±35 to 1500±40 AD and corresponds to the central point of the Spörer minimum that spans the period 1390-1550 AD (Fogtmann-Schulz et al., 2019; Marriner et al., 2022). This episode is weakly recorded at Aquileia, with a maximum anomaly of -0.09±0.14°C. Inversely, this phase is characterized by an important positive deviation in spring-summer precipitation, correlated with a catastrophic flood event in the nearby Isonzo River at

1480 AD (Siché, 2008) and a significant increase in precipitation in coastal Croatia (Kaniewski et al., 2021). This event is also correlated with a maximum frequency of sea storms in the Gulf of Venice (Camuffo et al., 2000). The last cold and wet episode recorded in AQ III fits with the Maunder minimum (1645-1715 AD; Shindell et al., 2001; Usoskin et al., 2015) that locally spans the period 1620 ± 30 to 1690 ± 30 AD. On average, the temperature anomaly is $-0.78\pm0.15^{\circ}\text{C}$ with a minimum of $-1.4\pm0.14^{\circ}\text{C}$ (Fig. 9A). The Maunder minimum is the second coldest episode and also the second wettest event, after the LALIA. The warmer phase is recorded from 1520 ± 40 to 1600 ± 30 AD, with an average annual temperature anomaly of $0.71\pm0.15^{\circ}\text{C}$. This warm period is correlated with a major increase in total solar irradiance during a phase of low solar activity (Steinhilber et al., 2009), and higher winter and summer temperatures in coastal Croatia (Kaniewski et al., 2021). The Eurasian summer temperature variability reconstructed from tree rings also depicts anomalies close to the MCA during this period (Büntgen et al., 2016). When the anthropogenic activities resumed at 1710 ± 35 AD under the Austrian Empire (Fig. 8C), the climate conditions were warm and still wet, facilitating agriculture and arboriculture. AQ III points to unstable environmental conditions in the northern Adriatic from 1250 ± 35 to 1770 ± 40 AD, with a maximum impact during the Maunder minimum. Even though AQ III is chronologically correlated with solar irradiance, a direct causal relationship is not suggested here because the cold LIA periods began earlier than the decline in solar activity and the Grand Solar Minimum.

6. Conclusions

The port city of Aquileia has provided a rare reconstruction of climatic and anthropogenic pressures on ecosystems from the end of the Roman Empire to the Austrian Empire in the northern Adriatic. The abandoned fluvial harbour evolved into a swamp, recording the major tipping points in the ecosystem dynamics, mainly due to climate pressures and, secondly, to anthropogenic activities. The main phases recorded by the ecosystems correspond to the LALIA and the Maunder minimum, with the development of cold and wet conditions. Inversely, the positive temperature anomalies reconstructed for the MCA suggest that this episode is close to temperatures recorded for the 20th century AD but, however, they differ from those of the 21st century AD. Anthropogenic activities, while diverse, seem to have been a secondary pressure at Aquileia. Their development is chronologically limited (late 7th to early 13th centuries AD) and their amplitude not strong enough to supersede the other environmental pressures. The long-term ecosystem changes that may correspond to human pressures on the rural environment

are probably masked by the climate dynamics. Aquileia suggests that the environmental pressures have been key in shaping the landscapes of the climate-sensitive northern Adriatic.

Author statement

Conceptualization: DK, NM, GS, DC, CM. Methodology: DK, NM, GS, DC, RC, TO, FL, CM. Investigation: DK, NM, GS, DB, MM, VR, AL, AB, MP, DC, MV, RC, TO, FL, CM. Visualization: DK, NM, GS, DC, CM. Funding acquisition: DK, NM, GS, DC, CM. Supervision: DK, NM, GS, DC, CM. Writing - original draft: DK, NM, GS, DC, CM. Writing - review & editing: DK, NM, GS, DB, MM, VR, AL, AB, MP, DC, MV, RC, TO, FL, CM.

Declaration of competing interest

The authors declare that they have no known competing financial interests or personal relationships that could have appeared to influence the work reported in this paper.

Acknowledgments

We wish to thank Daniele Pittaro for his support during the fieldwork campaign at Aquileia. The paper presents results of post-excavation laboratory analyses carried out as part of a wider project of archaeological and palaeoenvironmental research undertaken in the fluvial harbour of Aquileia (ex Fondo Sandrigo and adjacent areas) by the University of Venice Ca' Foscari, headed by D. Cottica, and under the auspices of the Italian Ministry of Culture in collaboration with the Soprintendenza Archeologia, belle arti e paesaggio del Friuli Venezia Giulia (Sabap FVG).

Data availability

All data needed to evaluate the conclusions in the paper are present in the paper and/or the Supplementary Materials (Raw data file).

Funding

Support was provided by the MITI CNRS “Événements rares”, AQUASANMARCO program, and the EPHE-DRI program. On-site research was funded by the Ca' Foscari University of Venice in collaboration with the Fondazione Aquileia.

References

- Allevato, E., Russo-Ermolli, E., Boetto, G., Di Pasquale, 2010. G. Pollen-wood analysis at the Neapolis harbour site (1st-3rd century AD, southern Italy) and its archaeobotanical implications. *Journal of Archaeological Science* 37, 2365-2375.
- Amorosi, A., Bini, M., Giacomelli, S., Pappalardo, M., Ribecai, C., Rossi, V., Sammartino, I., Sarti, G., 2013. Middle to late Holocene environmental evolution of the Pisa coastal plain (Tuscany, Italy) and early human settlement. *Quaternary International* 303, 93-106.
- Arnaud-Fassetta, G., Carre, M.B., Marocco, R., Maselli Scotti, F., Pugliese, N., et al., 2003. The site of Aquileia (northeastern Italy): example of fluvial geoarchaeology in a Mediterranean deltaic plain. *Géomorphologie : relief, processus, environnement* 9, 227-245.
- Arnaud-Fassetta, G., Carcaud, N., Castanet, C., Salvador, P.G., 2010. Fluvial palaeoenvironments in archaeological context: Geographical position, methodological approach and global change - Hydrological risk issues. *Quaternary International* 216, 93-117.
- Bini, M. et al. 2012. Palaeogeographies of the Magra Valley coastal plain to constrain the location of the Roman harbour of Luna (NW Italy). *Palaeogeography, Palaeoclimatology, Palaeoecology* 337-338, 37-51.
- Bini, M., Rossi, V., Amorosi, A., Pappalardo, M., Sarti, G., et al., 2015. Palaeoenvironments and palaeotopography of a multilayered city during the Etruscan and Roman periods: early interaction of fluvial processes and urban growth at Pisa (Tuscany, Italy). *Journal of Archaeological Science* 59, 197-210.
- Bondesan, A., Meneghel, M., Miola, A., Valentini, G., 2003. Palaeoenvironmental reconstruction from LGM to historical time in the lower coastal plain of the Piave river.

545 Preliminary pollen analysis on a 20 m core of lagoon and fluvial sediments. Italian Journal
546 of Quaternary Sciences 16, 121-130.

547 Bortolami, G.C., Fontes, J.C., Markgraf, V., Saliege, J.F., 1977. Land, sea and climate in the
548 northern Adriatic region during late Pleistocene and Holocene. Palaeogeography,
549 Palaeoclimatology, Palaeoecology 21, 139-156.

550 Büntgen, U., Tegel, W., 2011. European tree-ring data and the Medieval Climate Anomaly.
551 PAGES news 19, 14-15.

552 Büntgen, U., Myglan, V.S., Charpentier Ljungqvist, F., McCormick, M., Di Cosmo, N., et al.,
553 2016. Cooling and societal change during the Late Antique Little Ice Age from 536 to
554 around 660 AD. Nature Geoscience 9, 231-236.

555 Camuffo, D., Secco, C., Brimblecombe, P., Martin-Vide, J., 2000. Sea storms in the Adriatic
556 Sea and the western Mediterranean during the last millennium. Climatic Change 46, 209-
557 223.

558 Capulli, M., 2013. Ships of Aquileia. Underwater archaeological research on marine and inland
559 routes of the Upper Adriatic Sea. Skyllis - Zeitschrift für Unterwasserarchäologie 13, 18-
560 23.

561 Carre, M.B., 2008. Les fouilles du port fluvial d'Aquilée. Revue Archéologique - Nouvelle
562 Série 1, 193-198.

563 Cheddadi, C., Khater, C., 2016. Climate change since the last glacial period in Lebanon and the
564 persistence of Mediterranean species. Quaternary Science Reviews 150, 146-157.

565 Cheddadi, R., Araújo, M.B., Maiorano, L., Edwards, M., Guisan, A., et al., 2016. Thermal
566 niches of three European tree species during the last millennia. Frontiers in Plant Science
567 7, 1581. <https://doi.org/10.3389/fpls.2016.01581>

568 Cheddadi, R., Henrot, A.-J., François, L., Boyer, F., Bush, M., et al., 2017. Microrefugia,
569 climate change, and conservation of *Cedrus atlantica* in the Rif Mountains, Morocco.
570 Frontiers in Ecology and Evolution 5, 114. <https://doi.org/10.3389/fevo.2017.00114>

571 Cheddadi, R., Carré, M., Nourelbait, M., François, L., Rhoujjati, A., et al., 2021. Early
572 Holocene Greening of the Sahara requires Mediterranean winter rainfall. Proceedings of
573 the National Academy of Sciences, 118. <https://doi.org/10.1073/pnas.2024898118>

574 Cottica, D., Marchesini, M., Marvelli, S., Novello, M., Ventura, P., 2018. Per uno studio
575 integrato di uomo e ambiente ad Aquileia: alcune riflessioni a partire da recenti indagini
576 archeologiche. *Rivista di Archeologia* 41, 99-123.

577 Cottica, D., Ventura, P., 2019. Spunti per uno studio dell'interazione uomo e fiume in antico:
578 il caso della sponda orientale del Natiso cum Turro ad Aquileia. In: Auer, M. (Ed.),
579 Roman settlements along the Drava River. Harrassowitz Verlag, Wiesbaden, pp. 11-34.

580 Di Donato, V., Ruello, M.R., Liuzza, V., Carsana, V., Giampaola, D., et al., 2018. Development
581 and decline of the ancient harbor of Neapolis. *Geoarchaeology* 33, 542-557.

582 Di Rita, F., Magri, D., 2009. Holocene drought, deforestation and evergreen vegetation
583 development in the central Mediterranean: a 5500-year record from Lago Alimini
584 Piccolo, Apulia, southeast Italy. *The Holocene* 19, 295-306.

585 Di Rita, F., Lirer, F., Bonomo, S., Cascella, A., Ferraro, L., et al., 2018. Late Holocene forest
586 dynamics in the Gulf of Gaeta (central Mediterranean) in relation to NAO variability and
587 human impact. *Quaternary Science Reviews* 179, 137-152.

588 Divjak, A., 2013. The motif of warning birds in Attila's siege of Aquileia and its survival and
589 transformation in the *Origo civitatum Italiae seu Venetiarum* (*Chronicon Altinate et*
590 *Chronicon Gradense*), La Cronaca di Marco and Dandolo's *Chronica Extensa*. *Acta*
591 *Histriae* 21, 493-512.

592 Donnici, S., Serandrei-Barbero, R., Canali, G., 2012. Evidence of climatic changes in the
593 Venetian Coastal Plain (northern Italy) during the last 40,000 years. *Sedimentary*
594 *Geology* 281, 139-150.

595 Doyen, E., Vannière, B., Rius, D., Bégeot, C., Millet, L., 2015. Climate and biomass control on
596 fire activity during the late-glacial/early-Holocene transition in temperate ecosystems of
597 the upper Rhone valley (France). *Quaternary Research* 83, 94-104.

598 Faegri, K., Iversen, I., 1989. Textbook of pollen analysis, fourth ed. Wiley, London.

599 Finsinger, W., Tinner, W., 2005. Minimum count sums for charcoal concentration estimates in
600 pollen slides: accuracy and potential errors. *The Holocene* 15, 293-297.

601 Fogtmann-Schulz, A., Kudsk, S.G.K., Trant, P.L.K., Baittinger, C., Karoff, C., et al., 2019.
602 Variations in Solar Activity Across the Spörer Minimum based on Radiocarbon in Danish
603 Oak. *Geophysical Research Letters* 46, 8617-8623.

604 Fogtmann-Schulz, A., Baittinger, C., Karoff, C., Olsen, J., Knudsen, M.F., 2021. Radiocarbon
605 63, 91-104.

606 Hammer, Ø., Harper, D.A.T., Ryan, P.D., 2001. PAST: paleontological statistics software
607 package for education and data analysis. *Palaeontologia Electronica* 4. [http://palaeo-](http://palaeo-electronica.org/2001_1/past/issue1_01.htm)
608 [electronica.org/2001_1/past/issue1_01.htm](http://palaeo-electronica.org/2001_1/past/issue1_01.htm)

609 Henderson, P.A., 1990. Freshwater ostracods. In: Kermack, D.M., Barnes, R.S.K. (Eds.),
610 *Synopses of the British Fauna (New Series)*, vol. 42. Brill E.J., Leiden, pp.1-228.

611 Higuera, P.E., Brubaker, L.B., Anderson, P.M., Brown, T.A., Kennedy, A.T., et al., 2008.
612 Frequent fires in ancient shrub tundra: implications of paleorecords for arctic
613 environmental change. *PLoS ONE* 3, e0001744.
614 <https://doi.org/10.1371/journal.pone.0001744>

615 Higuera, P.E., Brubaker, L.B., Anderson, P.M., Sheng Hu, F., Brown, T.A., 2009. Vegetation
616 mediated the impacts of postglacial climate change on fire regimes in the southcentral
617 Brooks Range, Alaska. *Ecological Monographs* 79, 201-219.

618 Jones, P.D., Lister, D.H., Osborn, J., Harpham, C., Salmon, M., et al., 2012. Hemispheric and
619 large-scale land-surface air temperature variations: An extensive revision and an update
620 to 2010. *Journal of Geophysical Research* 117, D05127.
621 <https://doi.org/10.1029/2011JD017139>

622 Kaligarič, M., Culiberg, M., Kramberger, B., 2006. Recent vegetation history of the north
623 Adriatic grasslands: expansion and decay of an anthropogenic habitat. *Folia Geobotanica*
624 41, 241-258.

625 Kaniewski, D., Marriner, N., Morhange, C., Faivre, S., Otto, T. et al., 2016. Solar pacing of
626 storm surges, coastal flooding and agricultural losses in the Central Mediterranean.
627 *Scientific Reports* 6, 25197. <https://doi.org/10.1038/srep25197>

628 Kaniewski, D., Marriner, N., Morhange, C., Vacchi, M., Sarti, G., et al., 2018. Holocene
629 evolution of Portus Pisanus, the lost harbour of Pisa. *Scientific Reports* 8, 11625.
630 <https://doi.org/10.1038/s41598-018-29890-w>

631 Kaniewski, D., Marriner, N., Cheddadi, R., Morhange, C., Bretschneider, J., et al., 2019. Cold
632 and dry outbreaks in the eastern Mediterranean 3200 years ago. *Geology* 47, 933-937.

633 Kaniewski, D., Marriner, N., Cheddadi, R., Morhange, C., Cau Ontiveros, M.A., et al., 2020.
634 Recent anthropogenic climate change exceeds the rate and magnitude of natural Holocene
635 variability on the Balearic Islands. *Anthropocene* 32, 100268.
636 <https://doi.org/10.1016/j.ancene.2020.100268>

637 Kaniewski, D., Marriner, N., Cheddadi, R., Vacchi, M., Rovere, A., et al., 2021. Coastal
638 submersions in the north-eastern Adriatic during the last 5200 years. *Global and Planetary*
639 *Change* 204, 103570. <https://doi.org/10.1016/j.gloplacha.2021.103570>

640 Long, C.J., Whitlock, C., Bartlein, P.J., Millsaugh, S.H., 1998. A 9000-year fire history from
641 the Oregon Coast Range, based on a high-resolution charcoal study. *Canadian Journal of*
642 *Forest Research* 28, 774-787.

643 Lüning, S., Schulte, L., Garcés-Pastor, S., Danladi, I.B., Galka, M., 2019. The Medieval
644 Climate Anomaly in the Mediterranean Region. *Paleoceanography and Paleoclimatology*
645 34, 1625-1649.

646 Maggi, P., Maselli Scotti, F., Pesavento Mattioli, S., Zulini E., 2017. Lo scavo di Canale Anfora
647 (2004-2005). Editreg, Trieste.

648 Mann, M.E., Zhang, Z., Rutherford, S., Bradley, R.S., Hughes, M.K., et al., 2009. Global
649 signatures and dynamical origins of the Little Ice Age and Medieval Climate Anomaly.
650 *Science* 326, 1256-1260.

651 Mariotti Lippi, M., Bellini, C., Trinci, C., Benvenuti, M., Pallecchi, P., et al., 2007. Pollen
652 analysis of the ship site of Pisa San Rossore, Tuscany, Italy: the implications for
653 catastrophic hydrological events and climatic change during the late Holocene.
654 *Vegetation History and Archaeobotany* 16, 453-465.

655 Marriner, N., Morhange, C., 2006. The ‘Ancient Harbour Parasequence’: Anthropogenic
656 forcing of the stratigraphic highstand record. *Sedimentary Geology* 186, 13-17.

657 Marriner, N., Morhange, C., 2007. Geoscience of ancient Mediterranean harbours. *Earth-*
658 *Science Reviews* 80, 137-194.

659 Marriner, N., Morhange, C., Kaniewski, D., Carayon, N., 2014. Ancient harbour infrastructure
660 in the Levant: tracking the birth and rise of new forms of anthropogenic pressure.
661 *Scientific Reports* 4, 5554. <https://doi.org/10.1038/srep05554>

662 Marriner, N., Kaniewski, D., Pourkerman, M., Devillers, B., 2022. Anthropocene tipping point
663 reverses long-term Holocene cooling of the Mediterranean Sea: A meta-analysis of the
664 basin's Sea Surface Temperature records. *Earth-Science Reviews* 227, 103986.

665 Masari, F., Serandrei-Barbero, R., 2004. The environment of Venice area in the past two million
666 years. *Palaeogeography, Palaeoclimatology, Palaeoecology* 202, 273-308.

667 Mazzini, I., Faranda, C., Giardini, M., Giraudi, C., Sadori, L., 2011. Late Holocene
668 palaeoenvironmental evolution of the Roman harbour of Portus, Italy. *Journal of*
669 *Paleolimnology* 46, 243-256.

670 Mensing, S.A., Tunno, I., Sagnotti, L., Florindo, F., Noble, P., et al., 2015. 2700 years of
671 Mediterranean environmental change in central Italy: a synthesis of sedimentary and
672 cultural records to interpret past impacts of climate on society. *Quaternary Science*
673 *Reviews* 116, 72-94.

674 Michelangeli, F., Di Rita, F.D., Celant, A., Tisn rat-Laborde, N., Lirer, F., et al., 2022. Three
675 millennia of vegetation, land-use and climate change in SE Sicily. *Forests* 13, 102.
676 <https://doi.org/10.3390/f13010102>

677 Miola, A., Favaretto, S., Sostizzo, I., Valentini, G., Asioli, A., 2010. Holocene salt marsh plant
678 communities in the North Adriatic coastal plain (Italy) as reflected by pollen, non-pollen
679 palynomorphs and plant macrofossil analyses. *Vegetation History and Archaeobotany* 19,
680 513-529.

681 Morhange, C., Marriner, N., Carayon, N., 2016. Eco-history of ancient Mediterranean harbours.
682 In: Bekker-Nielsen, T., Gertwagen, R. (Eds.), *The Inland Seas, towards an eco-history of*
683 *the Mediterranean and the Black Sea*. Franz Steiner Verlag, Stuttgart, pp. 85-106.

684 Neukom, R., Steiger, N., G mez-Navarro, J., Wang, J., Werner, J.P., 2019. No evidence for
685 globally coherent warm and cold periods over the preindustrial Common Era. *Nature* 571,
686 550-554.

687 Ninfo, A., Fontana, A., Mozzi, P., Ferrarese, F., 2009. The map of Altinum, ancestor of Venice.
688 *Science* 325, 577.

689 Oldfield, F., Asioli, A., Accorsi, C.A., Mercuri, A.M., Juggins, S., et al., 2003. A high resolution
690 late Holocene palaeo environmental record from the central Adriatic Sea. *Quaternary*
691 *Science Reviews* 22, 319-342.

692 Osborn, T.J., Jones, P.D., 2014. The CRUTEM4 land-surface air temperature data set:
693 construction, previous versions and dissemination via Google Earth. *Earth System*
694 *Science Data* 6, 61-68.

695 Parshall, T., Foster, D.R., 2002. Fire on the New England landscape: regional and temporal
696 variation, cultural and environmental controls. *Journal of Biogeography* 29, 1305-1317.

697 Pederson, D.C., Peteet, D.M., Kurdyla, D., Guilderson, T., 2005. Medieval Warming, Little Ice
698 Age, and European impact on the environment during the last millennium in the lower
699 Hudson Valley, New York, USA. *Quaternary Research* 63, 238-249.

700 Peregrine, P.N., 2020. Climate and social change at the start of the Late Antique Little Ice Age.
701 *The Holocene* 30, 1643-1648.

702 Pini, R., Ravazzi, C., Donegana, M., 2009. Pollen stratigraphy, vegetation and climate history
703 of the last 215 ka in the Azzano Decimo core (plain of Friuli, north-eastern Italy).
704 *Quaternary Science Reviews* 28, 1268-1290.

705 R Core Team, 2021. R: A language and environment for statistical computing. R Foundation
706 for Statistical Computing, Vienna, Austria. URL <https://www.R-project.org/>.

707 Sadori, L., Giardini, M., 2007. Charcoal analysis, a method to study vegetation and climate of
708 the Holocene: The case of Lago di Pergusa (Sicily, Italy). *Geobios* 40, 173-180.

709 Sadori, L., Giardini, M., Giraudi, C. & Mazzini, I., 2010. The plant landscape of the imperial
710 harbour of Rome. *Journal of Archaeological Science* 37, 3294-3305.

711 Sadori, L., Allevato, E., Bellini, C., Bertacchi, A., Boetto, G., et al., 2015. Archaeobotany in
712 Italian ancient Roman harbours. *Review of Palaeobotany and Palynology* 218, 217-230.

713 Sadori, L., Giraudi, C., Masi, A., Magny, M., Ortu, E., et al., 2016. Climate, environment and
714 society in southern Italy during the last 2000 years. A review of the environmental,
715 historical and archaeological evidence. *Quaternary Science Reviews* 136, 173-188.

716 Salomon, F., Goiran, J.P., Noirot, B., Pleuger, E., Bukowiecki, E., et al., 2018. Geoarchaeology
717 of the Roman port-city of Ostia: Fluvio-coastal mobility, urban development and
718 resilience. *Earth-Science Reviews* 177, 265-283.

719 Shindell, D.T., Schmidt, G.A., Mann, M.E., Rind, D., Waple, A., 2001. *Science* 294, 2149-
720 2152.

- Siché, I., Forte, E., Prizzon, A., Arnaud-Fassetta, G., Fort, M., 2004. Cartographie hydrogéomorphologique et paléochenaux fluviaux en milieux profondément modifiés par les sociétés. L'exemple du port fluvial antique d'Aquilée dans la plaine du Frioul (Italie septentrionale, Adriatique). *Mosella* 29, 247-259.
- Siché, I., 2008. Migrations et métamorphoses historiques des fleuves torrentiels sur leur delta et leurs impacts sur les implantations portuaires antiques. L'exemple de l'hydrosystème Torre Natisone Isonzo sur la plaine côtière d'Aquilée (Méditerranée nord- occidentale). PhD thesis, Université Paris 7 Denis Diderot, France.
- Steinhilber, F., Beer, J., Frölich, C., 2009. Total solar irradiance during the Holocene. *Geophysical Research Letters* 36, L19704. <https://doi.org/10.1029/2009GL040142>
- Usoskin, I.G., Arlt, R., Asvestari, E., Hawkins, E., Käpylä, M., et al., 2015. The Maunder minimum (1645–1715) was indeed a grand minimum: A reassessment of multiple datasets. *Astronomy & Astrophysics* 581, A95. <https://doi.org/10.1051/0004-6361/201526652>
- Usoskin, I.G., Gallet, G.Y., Lopes, F., Kovaltsov, G.A., Hulot, G., 2016. Solar activity during the Holocene: the Hallstatt Cycle and its consequence for Grand Minima and Maxima. *Astronomy & Astrophysics* 587, A150. <https://doi.org/10.1051/0004-6361/201527295>
- Vannièrè, B., Colombaroli, D., Chapron, E., Leroux, A., Tinner, W., et al., 2008. Climate versus human-driven fire regimes in Mediterranean landscapes: the Holocene record of Lago dell'Accesa (Tuscany, Italy). *Quaternary Science Reviews* 27, 1181-1196.
- Yiou, P., Servonnat, J., Yoshimori, M., Swingedouw, D., Khodri, M., et al., 2012. Stability of weather regimes during the last millennium from climate simulations. *Geophysical Research Letters* 39, L08703. <https://doi.org/10.1029/2012GL051310>
- Zaccaria, C., Pesavento Mattioli, S., 2009. Uomini e merci. In: Ghedini, F., Bueno, M., Novello, M. (Eds.), *Moenibus at portu celeberrima Aquileia: Storia di una città*. Istituto Poligrafico e Zecca dello Stato, Roma, pp. 275-287.

Figures

Figure 1. Geographical location of the study area in Italy. The ancient harbour of Aquileia is marked in red. The city of Venice is indicated on the map by a green circle.

Figure 2. Focus on the core AQ III and the radiocarbon chronology. The lithology of the core is detailed according to depth. The sedimentation rates are shown in mm per year. The radiocarbon dates are depicted as intercepts and 2-sigma calibrations (95% of probability). The age model is compared and contrasted with linear (purple line) and polynomial (orange line) regressions.

Figure 3. Detailed pollen diagram (woody and herbaceous vegetation) for the period 500-1800 AD. The taxa are plotted on a linear age-scale. The vertical lines indicate the main transitions.

Figure 4. Detailed pollen diagram of the Aquileia river floodplain for the period 500-1800 AD. The taxa are grouped into PdVs and plotted on a linear age-scale. The vertical lines indicate the main transitions.

Figure 5. Pollen-based ecological clusters from Aquileia for the period 500-1800 AD. A cluster analysis (Paired group as algorithm, Correlation as similarity measure) was used to define the ecological assemblages. Each cluster was summed to create the PdVs. The PCA loadings of each PdV are indicated on the graph.

Figure 6. Environmental dynamics of the floodplain. (A) Evolution of the floodplain depicted by the riparian forest and marshland. The occurrence of hypohaline ostracods is also shown. (B) Loess PCA-Axis 1 (77% of total variance) shown with the 95% confidence band. (C) Pastoral activities alone (dark green) and pastoral activities with agriculture (light green) are plotted on a linear age-scale. All the long-term trends are highlighted by polynomial models (order 5, $P_{\text{value}} < 0.001$).

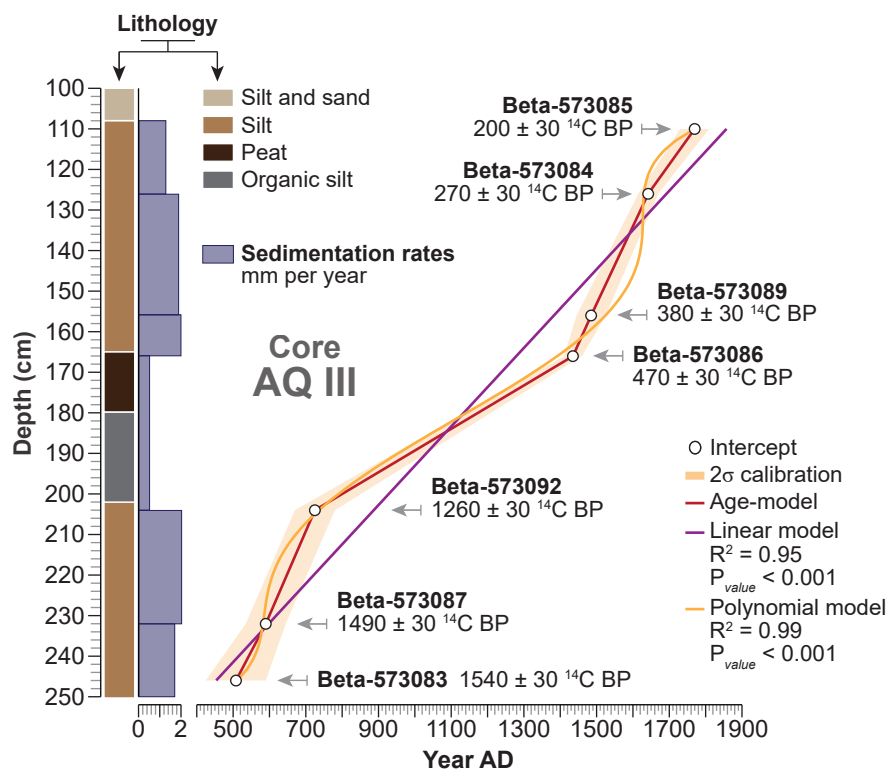
Figure 7. Floodplain dynamics compared and contrasted with dry components. (A) Variations in the floodplain contrasted with the dynamics of the dry floodplain scrubs based on

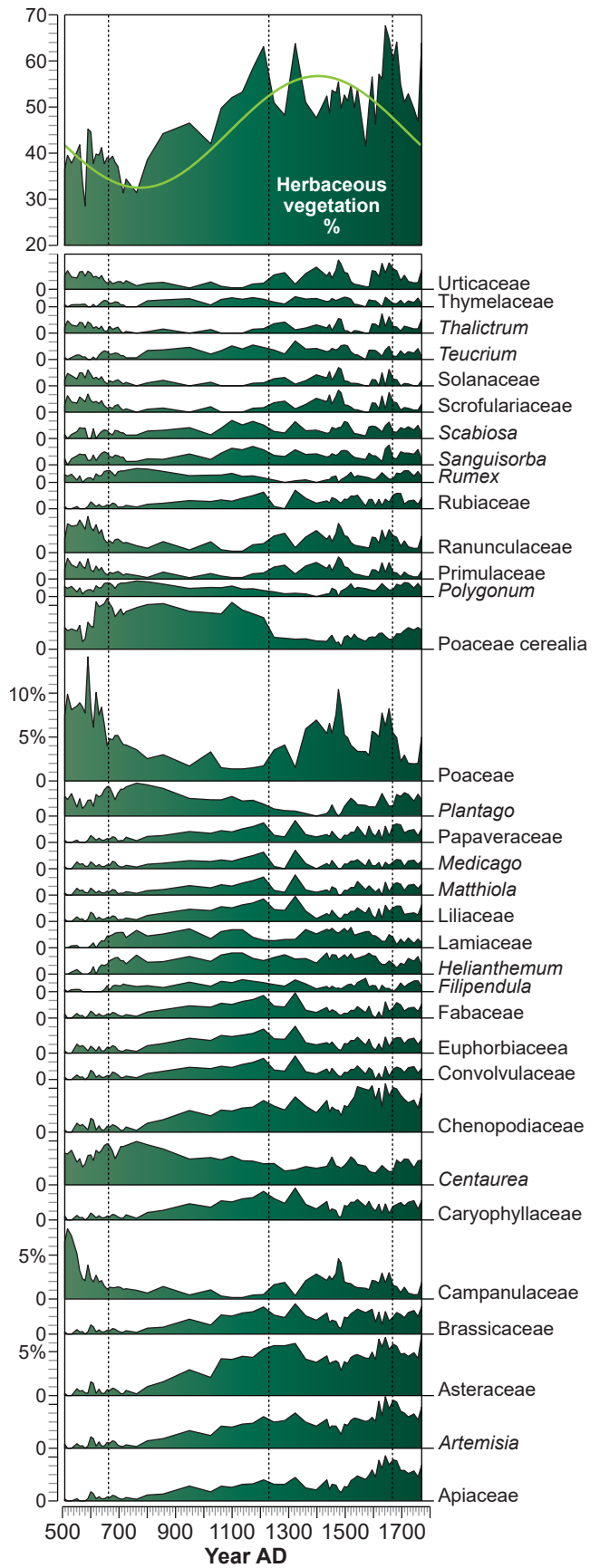
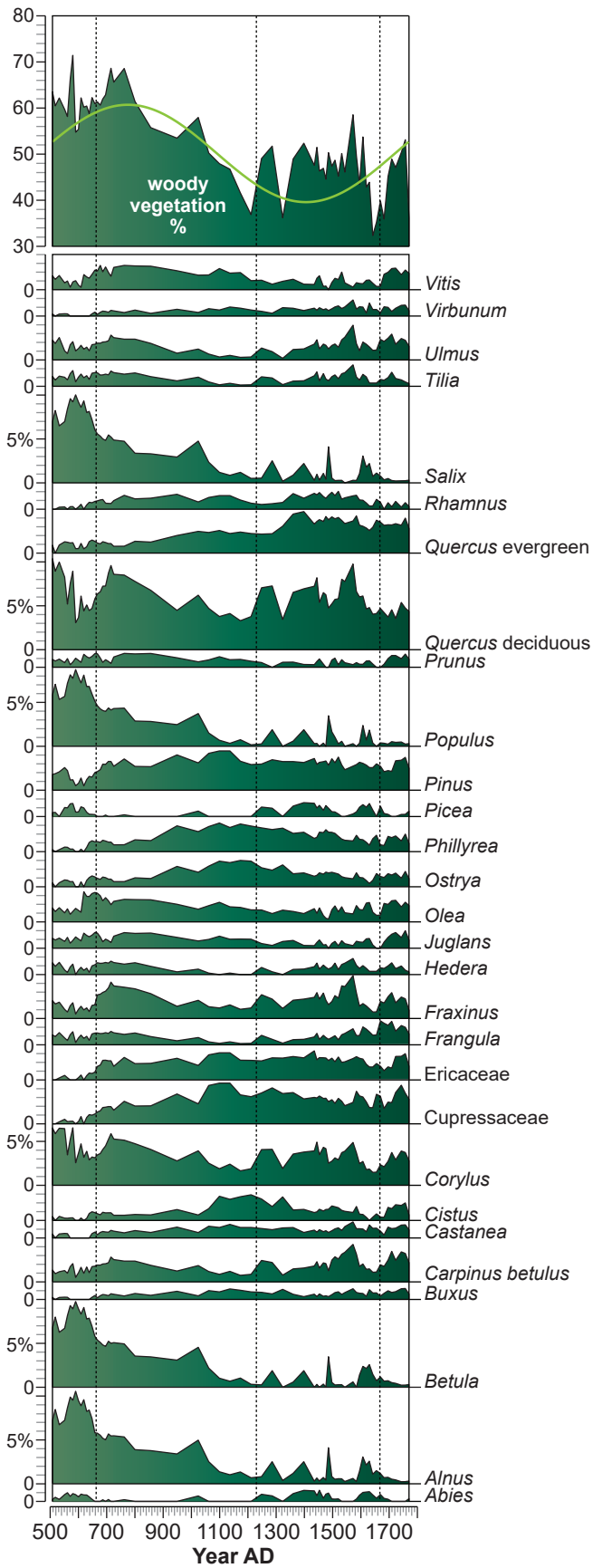
a synthetic diagram and a 2D Kernel-density model. The R^2 of the cross-correlation is indicated on the Kernel graph (B) Floodplain dynamic compared to the dryland components based on a synthetic diagram and a Generalized Linear Model. The R^2 of the cross-correlation is indicated on the synthetic diagram (C) Gradient Species packing test showing the distribution of each cluster taking the floodplain as a stationary reference. All the long-term trends are highlighted by polynomial models (order 5, $P_{\text{value}} < 0.001$).

Figure 8. Agriculture, pasture and fire activity. (A) Ratio pasture activities/agriculture and fire dynamics plotted on a linear age-scale. (B) Mixed oak forest dynamics compared and contrasted with fire activity (shown as a shaded curve). (C) Agro-pastoral activities contrasted with the fire activity (shown as a shaded curve). (D) CHAR analysis plotted on a linear age-scale. The red circles with white crosses denote the fire episodes. All the long-term trends are depicted by polynomial models (order 5, $P_{\text{value}} < 0.001$).

Figure 9. Pollen-based climate reconstruction. (A) Temperature anomalies (with the standard deviations) plotted on a linear age-scale. (B) Loess PCA-Axis 1 (77% of the total variance) shown with the 95% confidence band. (C) Spring-summer precipitation (with the standard deviations) plotted on a linear age-scale. All the long-term trends are depicted by polynomial models (order 5, $P_{\text{value}} < 0.001$). (D) Temperature anomalies compared and contrasted with the 1850-2019 CRUTEM4 data (Osborn and Jones, 2014). The sinusoidal model ($P_{\text{value}} < 0.001$) is depicted as a purple line.







Water

RIVER FLOODPLAIN

